

Effects of anthropogenic aerosols on temperature changes in China during the twentieth century based on CMIP5 models

Chunxiang Li¹ · Tianbao Zhao¹ · Kairan Ying¹

Received: 13 December 2014 / Accepted: 1 June 2015 / Published online: 14 June 2015
© Springer-Verlag Wien 2015

Abstract Using three models from the Coupled Model Inter-comparison Project Phase 5 (CMIP5), we compare the direct and other effects of anthropogenic aerosols on observed and simulated annual, winter, and summer temperature changes. Three regions, namely, arid–semiarid area, humid–semiarid area, and the whole of China, are studied. The temperature changes caused by other effects of anthropogenic aerosol (OE) are calculated from the difference between the anthropogenic aerosol forcing run (AA) and the anthropogenic aerosol direct effect forcing run (DE). When the combined effects are considered, a significant area-averaged cooling rate varies in the range of -0.86 to -0.76 °C per century throughout China. Meanwhile, the isolated direct and other effects lower the temperature nationwide by -0.66 to -0.55 °C per century, and -0.31 to -0.11 °C per century, respectively. From a non-linear perspective, the aerosol-induced temperature experiences a cooling trend, with AA having the largest cooling trend changes both annually and in the summer, while DE has the greatest reduction in the winter. Additionally, the influence of OE cannot be detected in observed annual changes over the arid–semiarid area and the whole of China, while the others are clearly detectable in all cases. AA (DE, OE) reduces the observational temperature mainly over the humid–semihumid region, where the contribution to the observed warming ranges from -515.2 % (-298.7 %, -198.9 %) to -173.6 % (-130.3 %, -66.4 %).

1 Introduction

Atmospheric aerosols influence the climate, both directly, through scattering and absorption of incoming short-wave solar radiation, and indirectly, through modification of the microphysics, radiative properties of clouds such as their albedo and lifetime (Charlson et al. 1992; Levine et al. 1995; Haywood and Boucher 2000). Aerosol direct and indirect effects can alter the net radiation both at the top and bottom of the atmosphere, thus modifying the atmospheric temperature structure. Meanwhile, climate changes triggered by aerosols are also enhanced by local feedbacks and modified by circulation changes (Koch et al. 2009). However, it is difficult to quantify these aerosol-driven effects (Haywood et al. 2003). Aerosol's indirect effects are especially difficult to quantify: the modification of cloud optical properties (e.g., the cloud albedo effect), structure, and precipitation (e.g., the cloud lifetime effect) by aerosols causes their influence to be the most uncertain radiative forcing in the climate system (Forster et al. 2007). Furthermore, the actual magnitude of the aerosol effect is the biggest uncertainty in the role of aerosols in climate, due to the complexity of the physical processes and lack of observations (Charlson et al. 1992; Shine et al. 1995).

In the past century, China experienced rapid population growth and industrial development, and became one of the world's major sources of anthropogenic atmospheric aerosol, especially those containing sulfur and carbon (Streets et al. 2003; Sun et al. 2013). Numerous studies have assessed the regional climate changes associated with anthropogenic aerosol emission, including changes in surface solar radiation trends, surface temperature and precipitation, and the summer monsoon (Xu 2001; Menon et al. 2002; Che et al. 2005; Zhao et al. 2006; Liu et al. 2011b; Jiang et al. 2013; Zhuang et al. 2013b). For instance, Giorgi et al. (2002,

✉ Tianbao Zhao
zhaotb@tea.ac.cn

¹ Key Laboratory of Regional Climate–Environment Research for East Asia, Institute of Atmospheric Physics, Chinese Academy of Sciences, 40 Hua Yan Li, Chao Yang District, Beijing 10029, China

2003) and Qian et al. (2003) investigated the regional climatic impacts of direct and indirect effects of anthropogenic aerosols over East Asia, and found that these effects go some way to explaining a cooling trend observed over various regions of China during the last decades of the twentieth century. Based on a regional coupled climate chemistry-aerosol model, Huang et al. (2006) concluded that the indirect effects of aerosol lead to a long-wave surface warming (+0.7 °C) at night and a daytime cooling (−0.7 °C) over the industrialized parts of China. Furthermore, Wang et al. (2010) investigated the direct and indirect effect of nitrate, one of the important components of aerosols, on temperatures in China, using the Regional Climate Chemistry Modeling System (RegCCMS). They demonstrated that changes in annual surface air temperature due to direct, first indirect, second indirect, and combined effects are −0.04, −0.11, −0.68, and −0.78 °C, respectively.

Even though there are extensive studies evaluating the direct and indirect effect of anthropogenic aerosol on temperature over China, few of those studies have assessed the effects on a multi-decadal or century scale using the CMIP5 historical experiments. Meanwhile, the influence of anthropogenic forcings has also been detected in certain types of extreme temperature events over China (Wen et al. 2013; Sun et al. 2014). However, no formal study has been conducted where the influence of anthropogenic aerosol was separated from that of other external forcings on long-term temperature changes over China. Therefore, this paper aims to quantitatively explore the direct and other effects of anthropogenic aerosol on linear and nonlinear temperature trends, as well as detect their contributions to observed temperature changes over China.

Characterized by fragile environmental conditions, including frequent and prolonged droughts and low and declining soil fertility, arid–semiarid regions are sensitive to both climate variability and human activities (Huang et al. 2012). It is significant to distinguish the impacts of anthropogenic aerosols over arid–semiarid areas from those on other climate regions. Based on the climatological data from Climatic Research Unit, the 500-mm isohyet of annual precipitation serves as a climatic boundary dividing China in two: the southeast portion is a humid–semihumid region, while the northwest portion is arid–semiarid (Fig. 1a). We analyze the effects of anthropogenic aerosols on surface air temperature changes in both the arid–semiarid and humid–semihumid areas, and across the whole country. The data used in the analysis, methods, and data processing are described in Section 2. The contributions of anthropogenic aerosol to temperature linear and nonlinear trends are discussed in Section 3, followed by the detection results in Section 4. Finally, Section 5 summarizes and discusses the results.

2 Datasets, methods, and data processing

2.1 Datasets

The observational precipitation and temperature are derived from CRU TS3.1 (Climatic Research Unit, University of East Anglia), which is available as monthly time series from 1901 to 2009 (Harris et al. 2014). We apply the former to define the climatic regions, while the latter to evaluate the performance of models and in the detection study. Meanwhile, the control simulations of 43 CGCMs (Table 1) from the Coupled Model Intercomparison Project Phase 5 (CMIP5; Taylor et al. 2012) are used to estimate the internal climate variability in the absence of external forcing. Among them, we further choose the models that include the historical experiments forced with: (1) combined natural and human external forcings (labeled ALL, following the CMIP5 metadata convention); (2) anthropogenic aerosol forcing (a mixture of aerosols, named AA); and (3) anthropogenic aerosol direct effect forcing (DE). Under these criteria, three models (CCSM4, GISS-E2-H, and GISS-E2-R) are selected. Table 2 lists the ensemble member and the specific external forcing agents used in each model. The ensemble mean of each model is given the same weight to construct the multi-model ensemble (MME) to estimate different forcing effects. The difference between AA run and DE run (the AA run minus the DE run) is taken to diagnose other effects of anthropogenic aerosol except DE, which we denote here by OE; hence, they include indirect, semidirect, surface albedo effects, and so on. This study mainly focuses on the 105-year period from 1901 to 2005.

2.2 Method

To explore the impacts of anthropogenic aerosols on the nonlinear trends of surface air temperature over China, the ensemble empirical mode decomposition (EEMD) method (Huang and Wu 2008; Wu and Huang 2009) is used to decompose the simulated temperature anomalies during the period 1901–2005. This is an adaptive and temporally local filter tool developed in recent years (Qian et al. 2011; Wu et al. 2011). In this study, the sum of the residual and the last Intrinsic Mode Function (IMF) are interpreted as a nonlinear trend, in order to filter out high frequency oscillatory modes while retaining multidecadal variability (Wilcox et al. 2013). Moreover, the derived trend provides time-varying information of the secular change of the raw data and is likely to reflect more accurately the physics behind the secular change than the linear trend (Qin et al. 2012).

Optimal fingerprinting has been widely applied for climate change detection and attribution (e.g., Zhang et al. 2007; Ribes et al. 2013; Sun et al. 2014). We use this technique to regress the observed spatio-temporal variations onto the model simulated patterns, using total least squares (tls) regression:

$$y = \beta x + \varepsilon$$

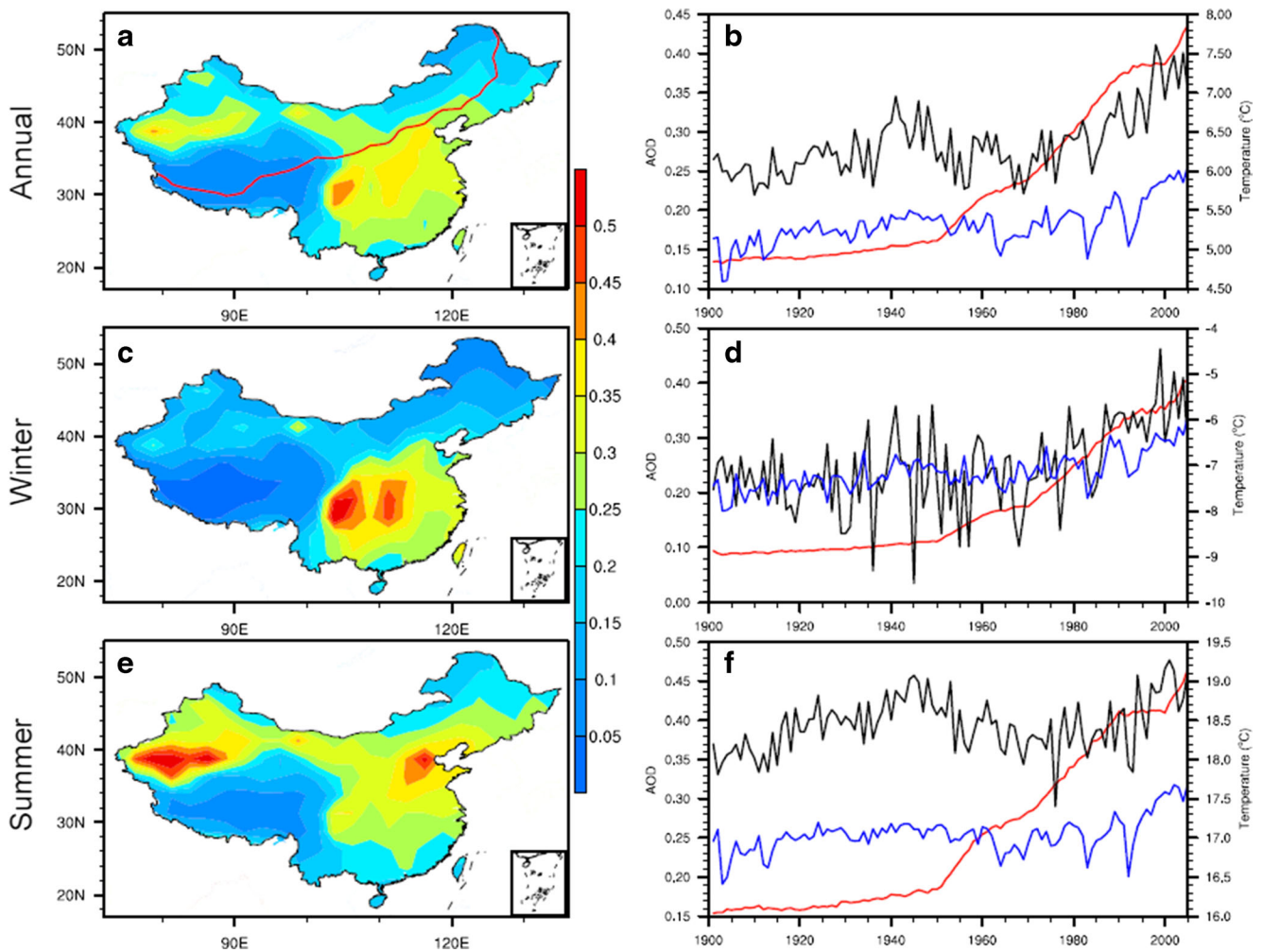


Fig. 1 Geographical distribution (*left panels*) of the 550 nm aerosol optical depth (AOD) from CMIP5 models in the period of 1901–2005: **a** annually, **c** in winter (December–February), and **e** summer (June–August). The evolution of nationwide averaged AOD (*red*), and observed (*black*) and simulated (*blue*) temperature is shown in the *right*

panels: **b** annually, **d** in winter, and **f** summer. The *red line* (500 nm isohyet) in **a** masks the boundary between the humid–semihumid and arid–semiarid areas. Note that only two of the three models (GISS-E2-H and GISS-E2-R) provide the AOD data for historical periods, which do not present stratospheric volcanic eruption as a change in AOD

where y is the observation, x denotes the climate response to the external forcing, β is an unknown scaling factor, and ε represents natural residual variability not explained by the signals. If the scaling factor exceeds zero at a particular significance level, a signal is detected in response to the imposed forcing, whereas the value consistent with unity implies a good match between model-simulated response and observed changes. A detailed theoretical discussion of the method can be found in Allen and Stott (2003). The residual consistency test (Ribes and Terray 2013) is passed for all results presented in Section 4.

2.3 Data processing

Prior to our analysis, both observations and model simulations are interpolated to a 5×5 grid via bilinear interpolation. Simulated data are masked by the observations to

ensure all temperature fields have the same coverage. The annual or seasonal temperature anomalies are computed relative to the 1961–1990 period, and then 5-year non-overlapping mean anomalies are calculated to reduce variability in the observations and noise in the signal data. A 105-year period thus provides 21 time steps. Next, the regional average is obtained to increase the signal/noise ratio, similar to the method of Stott et al. (2004). In total, 208 nonoverlapping 105-year segments are derived from the control simulations of the 43 models (Table 1). We split these in two: 104 samples are used to calculate the internal climate variability and the rest to estimate the uncertainty in the scaling factors. The method is carried out for the ensemble combining observations and model fingerprints from the ALL, AA, and DE runs constructed as time series of 5-year mean annual or seasonal temperature anomalies averaged over China during 1901–2005.

Table 1 List of CMIP5 control simulations used to estimate the internal climate variability and evaluate the uncertainty in the scaling factors

Model name	Length (years)	n_e	Model name	Length (years)	n_e
ACCESS1.0	500	4	FGOALS-s2	501	4
ACCESS1.3	250	2	GFDL-CM3	500	4
bcc-csm1-1	400	3	GFDL-ESM2G	500	4
bcc-csm1-1-m	500	4	GFDL-ESM2M	495	4
CanESM2	996	9	GISS-E2-H	251	2
CCSM4	1051	10	GISS-E2-H-CC	780	7
CESM1-BGC	500	4	GISS-E2-R	251	2
CESM1-CAM5	319	3	GISS-E2-R-CC	850	8
CESM1-FASTCHEM	222	2	HadGEM2-CC	240	2
CESM1-WACCM	200	1	HadGEM2-ES	576	5
CMCC-CESM	277	2	inmcm4	500	4
CMCC-CM	330	3	IPSL-CM5A-LR	1000	9
CMCC-CMS	500	4	IPSL-CM5A-MR	300	2
CNRM-CM5	359	3	IPSL-CM5B-LR	300	2
CNRM-CM5-2	850	8	MIROC5	670	6
COSMOS-ASO	400	3	MIROC-ESM	255	2
CSIRO-Mk3-6-0	500	4	MIROC-ESM-CHEM	630	6
CSIRO-Mk3L-1-2	1000	9	MPI-ESM-LR	1000	9
EC-EARTH	1353	12	MPI-ESM-MR	1000	9
FGOALS-g2	700	6	MPI-ESM-P	1156	11
FGOALS-s2	501	4	MRI-CGCM3	500	4
GFDL-CM3	500	4			

For each simulation, the name of the global coupled model, the length of the simulation used, and the number n_e of nonoverlapping 105-year segments derived from this simulation are indicated

3 Contributions to long-term trends

3.1 Spatial distributions of linear trends

Aerosol optical depth (AOD) is an optical property of an aerosol column that describes the extent to which aerosol scattering and absorption will attenuate solar radiation before it reaches the surface of the Earth (Guo et al. 2014). Generally, AOD is proportional to aerosol mass within the column, and thus, it is used here to estimate the temporal and spatial variation of aerosols. Figure 1 illustrates the spatial distribution of the annual and seasonal mean AOD over China (left panels)

and the corresponding area-averaged temporal variations (right panels). As indicated in Fig. 1, the distribution pattern of AOD over China is not nationally uniform and reveals seasonal variations: higher values are found during summer, whereas lower values are found during winter in most parts of China except for the Sichuan Basin and the middle and upper reaches of the Yangtze River. Meanwhile, in winter, the maximum values occur in Sichuan Basin where aerosol particles from local pollution sources could not diffuse well because of the frequent occurrence of calm wind and substantial water vapor suspended in the air due to the fog in the winter morning (Tao et al. 2014). During summer season, the AOD maximum

Table 2 The forcing agents in CMIP5 models

Model name	All forcing (ALL)		Anthropogenic aerosol (AA)		Anthropogenic aerosol direct effect (DE)	
	Rip code	Forcing agents	Rip code	Forcing agents	Rip code	Forcing agents
CCSM4	r[1–6]i1p1	SI, GHG, VI, SS, Ds, SD, BC, MD, OC, Oz, LU	r[1,4,6]i1p10	SS, Ds, SD, BC, MD, OC	r1i1p15	SD
GISS-E2-H	r[1–6]i1p1	Same as CCSM4	r[1–5]i1p107	SO2, BC, OC, NH3	r[1–5]i1p106	DE
GISS-E2-R	r[1–6]i1p1	Same as CCSM4	r[1–5]i1p107	SO2, BC, OC, NH3	r[1–5]i1p106	DE

SI solar, GHG greenhouse gases, VI volcanic aerosols, SS sea salt, Ds dust, SD sulfate direct effect, BC black carbon, MD mineral dust, OC organic black carbon, Oz ozone, LU land use change

centers exist in the northwestern part of China and the North China Plain, the former of which is likely due to sandstorms and floating dust and the latter is probably due to the low speed southwesterly summer monsoon winds and relative high humidity (Liu et al. 2011a, c).

There is a significant increase in nationwide averaged annual and seasonal AOD especially during the late period of the past century with the increased emission of anthropogenic aerosols. Meanwhile, both the observed and simulated temperature exhibits an upward trend, which is more evident in winter season. The spatial and temporal variations in AOD characteristics motivated us to examine the annual and seasonal mean contributions of anthropogenic aerosols over different regions in China.

The contribution of anthropogenic aerosol to surface air temperature is first investigated by considering the annual and seasonal linear trends over China in different forcing runs (Fig. 2). The observed annual temperature (Fig. 2a) displays that China underwent a significant warming trend, with a countrywide average of 0.85 °C per century during 1901–2005. The strongest warming is found in the arid–semiarid region (1.04 °C per century). This is consistent with previous studies, where the most intense increase in temperature occurs in arid–semiarid regions of the mid-latitude Northern Hemisphere (Ji et al. 2014). The warming signal, however, is much greater in boreal winter (0.96–1.78 °C per century) than summer (0.25–0.40 °C per century). Compared to the observations (Fig. 2a–c), all external forcing runs reproduce the general spatial features of temperature changes throughout China, with a slight underestimate in annual (0.41–0.73 °C per century) and winter (0.63–1.2 °C per century) changes, but an overestimate in summer (0.29–0.45 °C per century) (Fig. 2d–f).

The combined effect of anthropogenic aerosol (AA) induces a reduction by –0.86 to –0.73 °C per century in terms of domain and annual/seasonal average, with the largest decrease over the Tibetan Plateau adjacent to Sichuan Basin (Fig. 2g–i), where especially high aerosol loadings exist (see Fig. 1). Meanwhile, when only the direct effect is considered, the regional averaged cooling rate varies from –0.67 to –0.54 °C per century, with an effect more evident in the northeast during winter but near Shandong Province in the annual and summer mean. Unlike the direct radiative forcing, which is stronger in the eastern part of China, the significant cooling trends caused by OE concentrate in southwest China throughout the entire seasonal cycle. This is consistent with the results of studies on the secondary indirect effects of aerosol found by Wu and Han (2011). However, during winter, there is a slight warming trend over some regions in the north, most significantly in the far northeast, where large snow/ice cover exists (Shi et al. 2011, their Fig. 1a) and black carbon optical depth has increased significantly (see, e.g., Yang et al. 2014). This is probably due to the warming effect of the black carbon (BC)-snow albedo effect. In this process, deposition of BC on snow

or ice would reduce the surface albedo significantly, enhance melting, expose darker surfaces causing more melting and result in positive radiative forcing (warming) (Hansen and Nazarenko 2004; Jacobson 2004).

3.2 Annual cycle of anthropogenic aerosol contribution

To evaluate the effect of anthropogenic aerosol on the seasonal variation of temperature trends, we further present the regionally averaged trends (left panels of Fig. 3) and the percentage contributions of anthropogenic aerosol to the total trends in the ALL runs (right panels of Fig. 3) in each calendar month for the arid–semiarid area, humid–semihumid area, and the whole of China. A “contribution” is defined as the ratio of trend in anthropogenic aerosol single forcing runs (AA, DE, and OE) to the trend in all forcing runs.

Trends in the three regions (left panels) show a large seasonal cycle, with a minimum increase in observation and the ALL run, and a maximum decrease in aerosol forcing runs found in summer (August or September). The models duplicate the seasonality of observation, but overestimate the observed warming trend during July–October while underestimate it during the rest of the year. More specifically, for the arid–semiarid region (Fig. 3a, b), the observed warming varies from 0.18 (August) to 1.95 °C per century (February), and the simulated trend ranges from 0.35 (June) to 1.39 °C per century (December). Meanwhile, the trends under AA forcing are negative (–0.98 to –0.44 °C per century), reaching the maximum during summer and explaining the –207 to –47 % to the simulated warming in the ALL runs. If only the direct effect is considered, the cooling trends are reduced to –0.79 to –0.29 °C per century, accounting for –134 to –40 % of the trends in the ALL runs. However, the OE cools this region by –0.43 to –0.02 °C per century in all months, except for March (0.12 °C per century), accounting for –91 to 16 % in the ALL trends. This warming in March is likely to be associated with the BC-snow albedo effect, which is strongest during local springtime (see, e.g., Hall and Qu 2006; Flanner et al. 2007), when a large portion of the arid–semiarid region is snow-covered and exposed to intense insolation. Comparison of DE and OE reveals that the response of surface air temperature to anthropogenic aerosol is dominated by the direct effect in all months (53–127 %) except November (48 %).

In comparison with the arid–semiarid region, the area-averaged warming rate of the humid–semihumid region is much smaller in all months, both presented in observations (0.02–1.31 °C per century) and the ALL runs (0.25–0.74 °C per century). However, the magnitudes of aerosol-induced cooling are close to those of the arid–semiarid region (Fig. 3c). Consequently, the contribution of anthropogenic aerosol (–328 to –112 %), including direct (–212 to –55 %) and other effects (–132 to –3 %), to the simulated warming trend is much greater, especially in summer and autumn

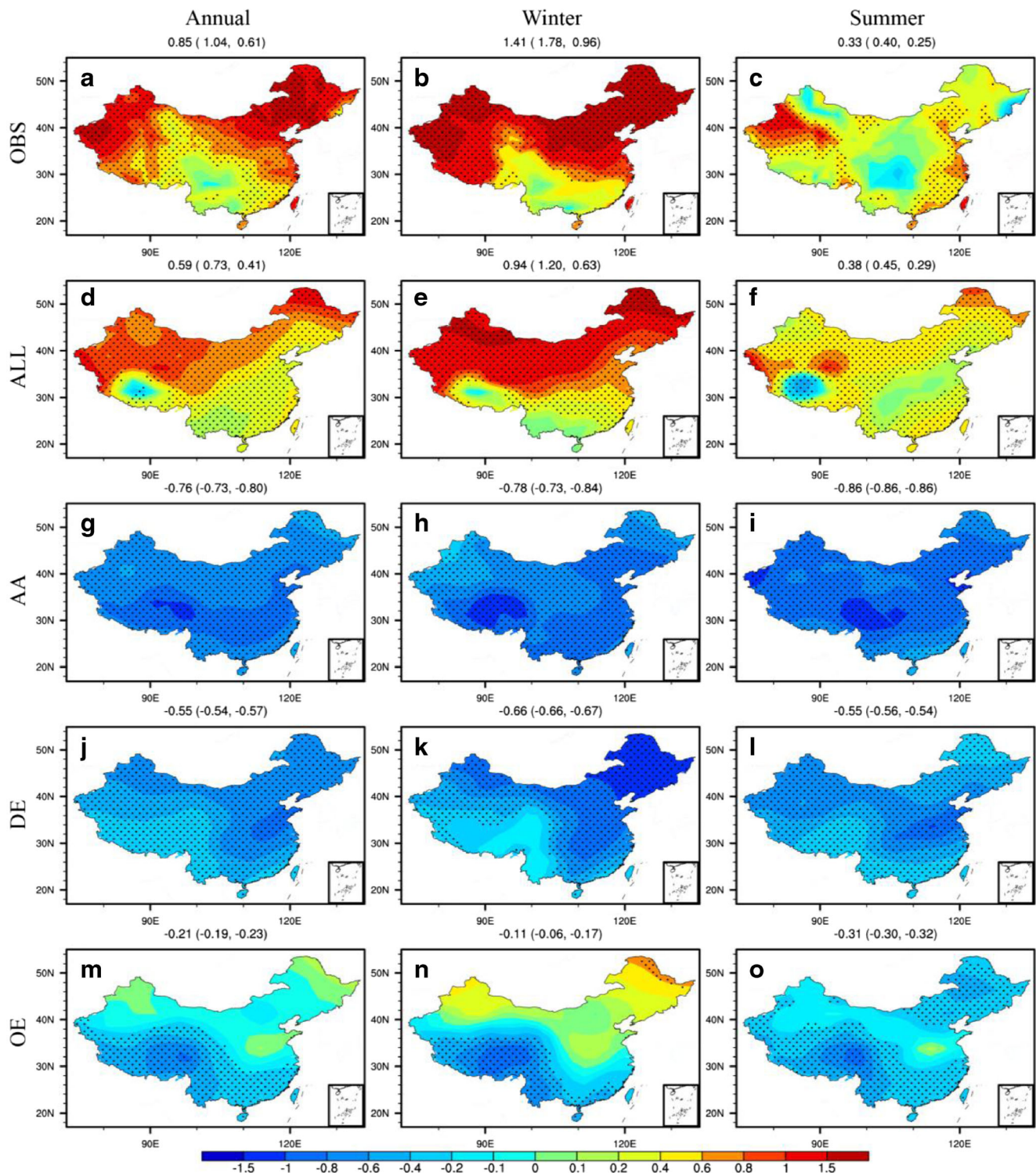


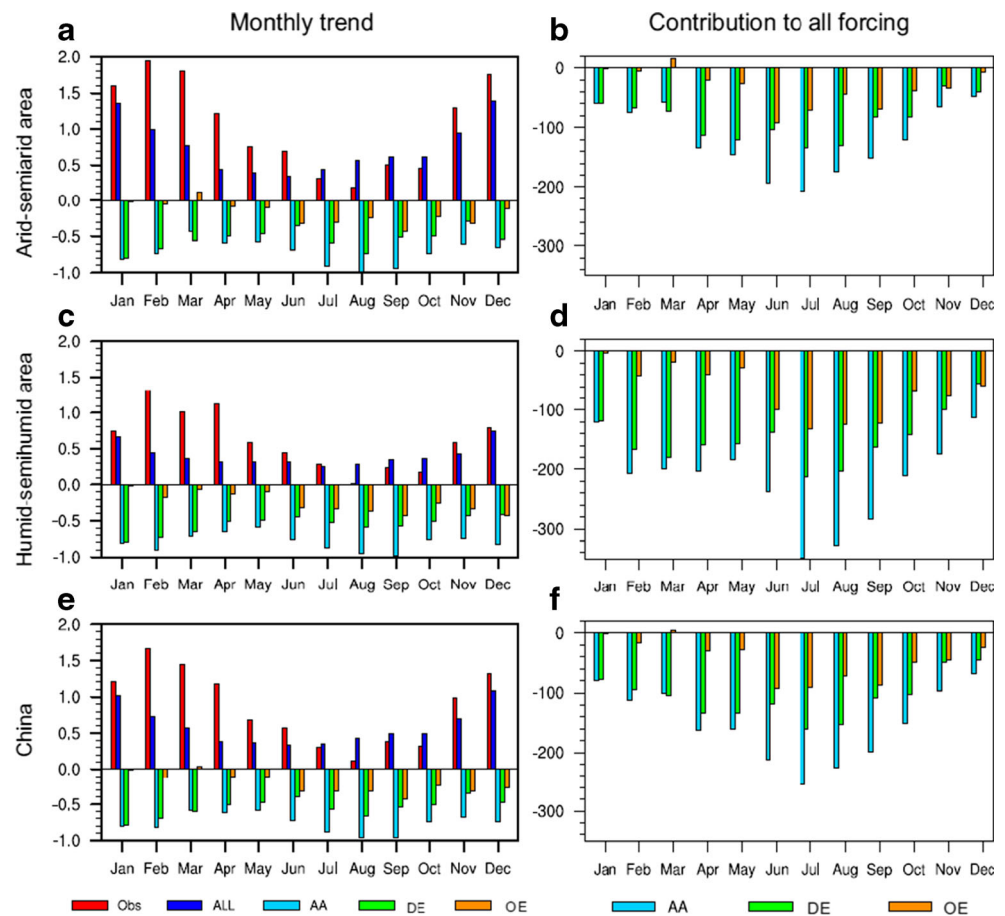
Fig. 2 Geographic distribution of trends ($^{\circ}\text{C}$ per century): annually (*left panels*), in winter (*middle panels*), and summer (*right panels*). Mean temperatures are **a–c** observations, **d–f** ALL, **g–i** AA, and **j–l** DE runs, and **m–o** the difference between AA and DE runs (OE). Model output and observation are from January 1901 to December 2005. The values

displayed in the figure panels are area-averaged trends in the whole of China, arid–semiarid, and humid–semihumid regions (in *brackets*), respectively. Stippling represents statistically significant trends at a 95 % confidence in interval based on a two-tailed Student’s *t* test

(Fig. 3d). For the countrywide averages, the contribution values of AA (DE, OE) are between the values for the arid–semiarid

and humid–semihumid regions with magnitudes varying from -254% (-160% , -94%) to -69% (-44% , 5%).

Fig. 3 The seasonal cycle in the arid–semi-arid area (*top panels*), humid–semi-humid area (*middle panels*), and the whole of China (*bottom panels*) for the averaged trends (*left panels*; units, °C per century) and for the individual contributions to the trends of the ALL forcing runs (*right panels*; units, %). Model output and observation are from January 1901 to December 2005



3.3 Nonlinear trends

In this study, we focus on the impact of anthropogenic aerosol on surface air temperature long-term secular changes over China since 1901. All the analyses above are based on linear trends, which can extract the warming or cooling only at a constant rate. As warming or cooling over different regions is not uniform with time, such time invariant change may not effectively reveal the true nature of climate change and variability (Ji et al. 2014). To address the problem and deepen understanding of the temperature change in the past century, the residual and last IMF obtained from the EEMD are used to reconstruct the nonlinear trend. The nonlinear trends of annual, winter, and summer mean temperature over the arid–semi-arid region as well as the percentage contributions from each anthropogenic aerosol forcing to the overall forcing trend in time are illustrated in Fig. 4.

For the annual mean temporal evolution in the arid–semi-arid area of China (Fig. 4a), observations show a slight cooling trend until 1915, a slow warming until 1970, and the warming shifts robustly after that. Before 1985, the warming trends obtained from the ALL runs are superior with observations and get inferior after that. There are consistent cooling trends shown both in AA and DE forcing runs, which are

otherwise close before 1955. Correspondingly, a weak cooling trend is found in OE until after 1955. Figure 4b shows a clear turning point of contributions around 1980, from increasing to decreasing in the magnitude of the negative contributions, depicted in the three aerosol forcing runs. More specially, the negative contribution of AA increases from -18 to -101 % until 1980, then gradually decreases to -57 %. The direct effect triggers a similar evolution to that of AA, except for a short-term decrease in the early period of the twentieth century. However, the contribution of the OE shows a decrease until 1936 (from -28 to -0.3 %), a small positive value during 1937–1945, an increasingly negative value until 1980, and finally a decrease until 2005.

For the winter temperature, there is an observed transition from a slowly decreasing trend to a rapidly increasing trend occurring around 1965 (Fig. 4c), whereas warming in summer has slowed since then (Fig. 4e). Meanwhile, the simulated temperature in the ALL runs has a warming trend during 1901–1945; however, it has a cooling trend after 1945 and resumes a warming trend after 1970, exhibiting a similar evolution to those of annual and summer temperature changes (Fig. 4a, e). AA and DE have a cooling trend, while no significant trend is found in OE throughout the entire period. At the beginning of the twentieth century, the contributions of

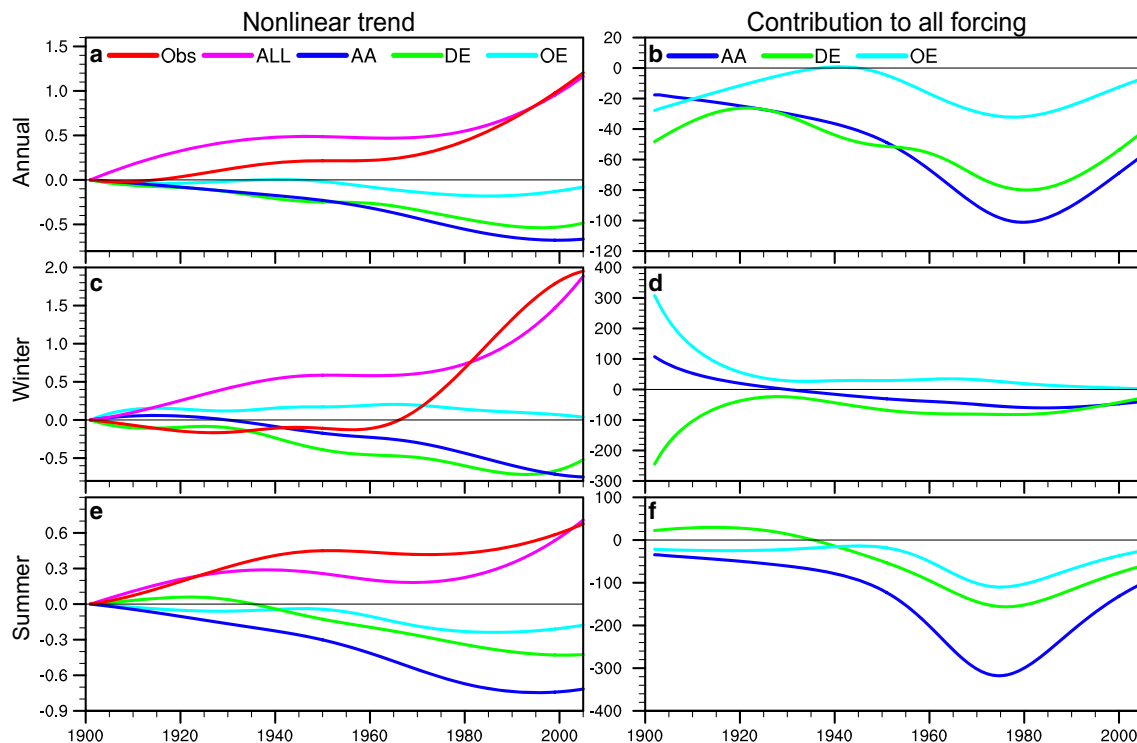


Fig. 4 Nonlinear trend [the sum of the last intrinsic mode forcing (*IMF*) and the residual obtained through an empirical ensemble mode decomposition (*EEMD*)] from observations, ALL forcing runs, and single forcing runs for area-averaged **a** annual-mean, **c** winter season (DJF), and **e** summer season (JJA) temperature in the arid–semiarid area.

Contributions from combined (*AA*), direct (*DE*), and other (*OE*) effects of anthropogenic aerosol to the nonlinear trend in ALL forcing runs are shown in **b** annual-mean, **d** winter season (DJF), and **f** summer season (JJA) temperature

AA, DE, and OE to the nonlinear trends of ALL fall sharply and remain stable after 1925. It should be noted that the contribution of AA decreases monotonically from 107 to -61% before 1984, and increases gradually to -40% from then on. However, the contribution of OE is positive during the whole period, ranging from 2 to 307%, exhibiting a promotion to the simulated warming trends in the winter.

The summer mean temperature shows a similar characteristic in the evolution of nonlinear trends and contributions to the annual mean. However, two differences are worthy of note. First, the magnitude of nonlinear trends, both in the observation and the ALL runs, is smaller to that of annual temperature. Thus, greater contributions are obtained in summer. Second, the contribution extremes appear around 1975 so the maximum effect of anthropogenic aerosol on nonlinear temperature trends are found close to 1975 in summer, but at the beginning of the period in winter and at around 1980 in the annual mean.

In general, both the trends of observation and the ALL simulation correspond to warming trends, with the largest warming found in the ALL runs at the beginning of the twentieth century, but in the late twentieth century for observation. Meanwhile, the time series in anthropogenic aerosol forcing runs experience a cooling trend, with the AA exhibiting the largest cooling in annual and summer mean temperature,

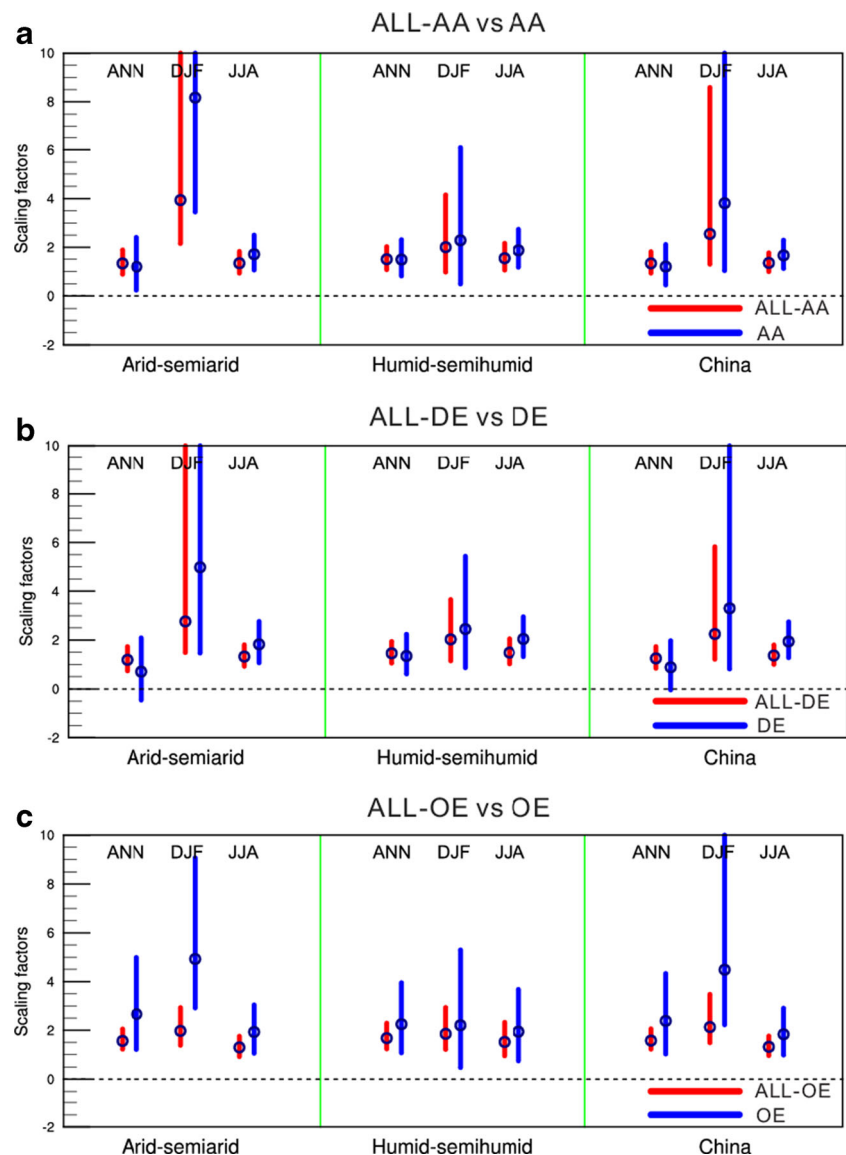
while DE has its greatest reduction in winter. For the annual mean nonlinear trends, the negative contributions of AA, DE, and OE increase in magnitude from -18 , -48 , and -27 to -101 , -80 , and -41 until 1980, but then decrease to -57 , -41 , and -6% after 1980, respectively. Similar results are found in the contributions in the summer, whereas OE promotes the simulated warming trends in the winter.

When it comes to the regional dependency, the general evolutions of nonlinear trends and contributions of aerosols in the humid–semihumid region and the whole of China (figures are omitted) are approximately similar to those in the arid–semiarid region. Nevertheless, a distinct difference of winter mean temperature among the humid–semihumid region, the whole of China, and arid–semiarid region should be noted. In the former two areas, the contributions of OE in winter decrease monotonically from positive to negative, with a turning point in the late 1980s. In the latter region, the contribution of OE falls sharply at first, but remains positive during the entire period. The results illustrate that OE enhances the simulated winter warming trend in the ALL runs before 1980s, but suppresses afterwards over the humid–semihumid area, and the whole of China. However, OE favors the nonlinear trend in winter over the arid–semiarid area during the past century, especially at the beginning of the period.

4 Results of detection

The results from the optimal fingerprinting analysis for each season and each domain are discussed individually, based on two-signal analysis of regressing the observed spatio-temporal variations onto the two model-derived response patterns from AA (DE, OE) and ALL-AA (ALL-DE, ALL-OE). It attempts to partition the relative contributions of AA and ALL-AA, DE and ALL-DE, and OE and ALL-OE to the observed response, respectively. Here, ALL-AA (ALL-DE, ALL-OE) represents the difference between ALL and AA (or DE, OE), thus indicating the temperature response to all the external forcings except AA (or DE, OE), which is dominated by the effects of greenhouse gases. Scaling factors for seasonal and annual changes over the three domains and their 5–95 % uncertainty ranges are depicted in Fig. 5.

Fig. 5 Scaling factor best estimates (*circles*) and their 90 % confidence intervals (*solid lines*), as estimated in a two-signal forcing analysis for **a** ALL-AA and AA, **b** ALL-DE and DE, and **c** ALL-OE and OE forced simulation-based fingerprints over the arid–semiarid region (*left panel*), the humid–semihumid region (*middle panel*), and the whole of China (*right panel*). Results are given for annual (*ANN*), winter (*DJF*), and summer (*JJA*) temperature changes of the ensemble of the three models, respectively



In all cases, the scaling factors for ALL-AA and AA forcings are consistently greater than zero (Fig. 5a), indicating that both ALL-AA and AA signals are detectable in the observed temperature changes and their influence can be distinguished from China random climate variability. Moreover, for the winter temperature over the arid–semiarid region, both of ALL-AA and AA responses are underestimated, while their uncertainty ranges encompass unity for the other cases, suggesting that their signal amplitudes are consistent with the observation. Meanwhile, the detection of the ALL-DE response pattern occurs in all cases. In contrast, the response to the direct effect of anthropogenic aerosol is not robustly detected in annual changes over arid–semiarid region or the whole of China (Fig. 5b). The detection results obtained from ALL-OE and OE (Fig. 5c) are quite similar to those from ALL-AA and AA (Fig. 5a). That is, both the ALL-OE and OE forcings are found to be significantly positive in all cases,

implying that they significantly contribute to observed temperature changes. Moreover, the model simulated responses to OE and ALL–OE in most cases are smaller than observed.

Analysis for annual or seasonal temperature changes conducted with ALL–AA against AA, ALL–DE against DE, and ALL–OE against OE suggests that the effect of anthropogenic aerosol, especially the OE, can be separated from those of other external forcings. Meanwhile, all the scaling factors are found to be significantly greater than unity in the winter temperature changes over arid–semiarid region, indicating that the response amplitudes of all the forcings are smaller than the observation. With respect to other forcings, the scaling factors of AA (DE, OE) are much farther to unity with wider uncertainty ranges for any season or for annual changes over the three domains, indicating that observed changes are less attributable to AA (DE, OE).

Table 3 shows anthropogenic aerosol (AA, DE, and OE) induced temperature changes and the corresponding contributions to the observed changes for the whole period. Over the arid–semiarid area, the net cooling from the combined anthropogenic aerosol forcing is -1.01 °C (-2.97 °C, -1.21 °C), thereby offsetting -91 % (-158 %, -277 %) of the observed annual (winter, summer) warming. Meanwhile, the direct and other effects contribute -0.68 and -0.29 °C (-1.95 and -0.1 °C, -0.78 and -0.4 °C) to the observed annual (winter, summer) changes, which are -61 and -26 % (-103 and -5 %, -178 and -92 %) of the observed warming. For humid–semihumid region, the AA-induced decrease is -1.27 °C (-0.85 °C, -0.43 °C), contributing -195 % (-174 %, -515 %) to the observed annual (winter, summer) changes. The detectable contributions of DE to the observed annual (winter, summer) temperature changes increase to -130 % (-135 %, -299 %), which goes some way to explain the cooling effect of anthropogenic aerosols, especially in the winter season. The AA (DE, OE) produces a nationwide decrease in annual temperature of -1.07 °C (-0.72 °C, -0.35 °C), with a peak in winter by -2.08 °C (-1.55 °C, -0.27 °C). It has been suggested that the responses of mean temperature due to the anthropogenic aerosol forcings are greater in winter than in summer (e.g., Shiogama et al. 2006).

For the regional discrepancy, the contributions of anthropogenic aerosols, despite direct and other effects over the humid–semihumid region, are much stronger than those in the arid–semiarid region, consistent with the simulated distribution of anthropogenic aerosols found by Zhuang et al. (2013a). For seasonal changes, the cooling magnitude induced by AA (DE, OE) in summer is smaller than that in winter, while the contributions are much larger due to the weaker observed increase in summer. In general, although the detection of DE fails in the annual changes over the arid–semiarid region and the whole of China, the cooling effect of anthropogenic aerosols is mainly attributable to the direct effects, especially in winter.

5 Summary and discussion

By analyzing historical simulations from three CMIP5 models, we found that widespread areas in China have undergone a significantly observed warming trend (0.33 – 1.41 °C per century), with the strongest increase in the arid–semiarid region (0.40 – 1.78 °C per century). The anthropogenic aerosols, including AA, DE, and OE, lowered temperatures almost everywhere in China, with a nationwide average of -0.86 to -0.76 °C per century, -0.66 to -0.55 °C per century, -0.31 to -0.11 °C per century, respectively. However, the slight warming is found over the north portion during winter in OE runs, which may be due to effects of aerosol on snow albedo, where aerosol deposition reduces snow albedo. In addition, the AA-forced long-term temperature trends showed a clear seasonal cycle in the three domains, with a maximum aerosol-induced reduction in temperature appearing in summer. For the arid–semiarid area, the ratios of AA- (DE- and OE-) driven cooling trends could account for the simulated changes, about -207 % (-134 %, -91 %) to -47 % (-40 %, 16 %) in the ALL runs. Over the humid–semihumid region, the suppression of anthropogenic aerosol (-328 to -112 %), in conjunction with DE (-212 to -55 %) and OE (-132 to -3 %), to the warming trends are much greater, especially in the warm season. For the whole country, the contributions of AA (DE, OE) to the long-

Table 3 Anthropogenic aerosol-induced 105-year temperature changes and their contributions to the observed changes (italics in brackets), including direct and other effects

Region	Arid–semiarid			Humid–semihumid			Whole of China		
	AA	DE	OE	AA	DE	OE	AA	DE	OE
Annual	-1.01 (<i>-91</i>)	-0.68 (<i>-61</i>)	-0.29 (<i>-26</i>)	-1.27 (<i>-195</i>)	-0.85 (<i>-130</i>)	-0.43 (<i>-66</i>)	-1.07 (<i>-120</i>)	-0.72 (<i>-81</i>)	-0.35 (<i>-39</i>)
Winter	-2.97 (<i>-158</i>)	-1.95 (<i>-103</i>)	-0.10 (<i>-5</i>)	-1.77 (<i>-174</i>)	-1.37 (<i>-135</i>)	-0.38 (<i>-38</i>)	-2.08 (<i>-142</i>)	-1.55 (<i>-106</i>)	-0.27 (<i>-18</i>)
Summer	-1.21 (<i>-277</i>)	-0.78 (<i>-178</i>)	-0.40 (<i>-92</i>)	-1.40 (<i>-515</i>)	-0.81 (<i>-299</i>)	-0.54 (<i>-199</i>)	-1.22 (<i>-342</i>)	-0.77 (<i>-217</i>)	-0.44 (<i>-123</i>)

Value in bold shows where forcing is not detected. The simulated changes are estimated as linear changes multiplied by corresponding scaling factors obtained from ALL–AA and AA, ALL–DE and DE, and ALL–OE and OE two-signal analysis. The results shown are the annual, winter, and summer means over the arid–semiarid region, the humid–semihumid region, and the whole of China, respectively

term temperature changes in the ALL runs range from -254% (-160% , -94%) to -69% (-44% , 5%).

In terms of nonlinear trend, there is a cooling trend of the aerosol-driven temperature, with the AA exhibiting the largest cooling in the annual and summer mean, while the DE had the greatest reduction in the winter. Meanwhile, the negative contributions of AA, DE, and OE increased before the 1980s, followed by a decrease after the 1980s in all seasons except winter evolution in OE. That is, in winter, the other effects of anthropogenic aerosol promote the warming trend simulated in the ALL runs before the 1980s and suppress it afterwards, over the humid–semihumid area and the whole of China. Meanwhile, it favors the nonlinear trend over the arid–semiarid area throughout the century, especially at the beginning of that period.

Furthermore, the influences of anthropogenic aerosol and other external forcings on the observed changes over different regions are assessed by optimal fingerprinting analysis. We separated the contributions of anthropogenic aerosol (including DE and OE) cooling and the warming due to other forcings to the annual and seasonal temperature changes over the three domains, with the exceptions of the annual changes over arid–semiarid area and the whole of China. For the contribution to the observed annual and seasonal changes, about -272 to -91% of the observed warming over arid–semiarid region was offset by the combined negative effect of anthropogenic aerosol, where -178 to -61% was caused by DE and -92 to -5% is due to OE. Meanwhile, the simulated contribution of AA (DE, OE) increased to -515% to -174% (-299% to -130% , -199% to -66%) over the humid–semihumid area. Therefore, the nationwide average of AA (DE, OE) contributions was between those of the two sub-regions.

In general, the effects of anthropogenic aerosol on the long-term temperature changes based on the CMIP5 simulations in this work are qualitatively similar to previous studies. However, some limitations are worth noting. The primary limitation of this work is the lack of additional experiments only forced by other effects, such as indirect and semidirect effects, of anthropogenic aerosols. As described above, we crudely take the differences between AA and DE as the other effects of anthropogenic aerosol, under the assumption of linearly additive responses to the external forcings. However, additivity may not continue to hold well on regional scales, and biogeochemical feedback mechanisms may cause nonadditive feedbacks to radiative forcing (Cox et al. 2000). In future work, the isolated indirect and semidirect effect of anthropogenic aerosol remains to be further investigated by single forcing simulations. Additionally, CMIP5 models still have certain limitations regarding aerosol–cloud and aerosol–radiation interaction representation at a regional scale, and there are large uncertainties among models in terms of aerosol burden, and as to what types of aerosol are considered important. In this study, this is manifested as larger uncertainty ranges in the detection analysis. Therefore, the simulated results in this

paper need to be tested and confirmed by more complex physically-based climate models.

Acknowledgments We appreciate the valuable suggestions from the anonymous reviewers. This work was supported by grants from the National Basic Research Program of China (2012CB956203), Open Research Fund Program of Plateau Atmosphere and Environment Key Laboratory of Sichuan Province (PAEKL-2015-C1), and the National Natural Science Foundation of China (41405090).

References

- Allen MR, Stott PA (2003) Estimating signal amplitudes in optimal fingerprinting, part I: theory. *Clim Dyn* 21:477–491
- Charlson RJ, Schwartz SE, Hales JM et al (1992) Climate forcing by anthropogenic aerosols. *Science* 255:423–430
- Che HZ, Shi GY, Zhang XY et al (2005) Analysis of 40 years of solar radiation data from China, 1961–2000. *Geophys Res Lett* 32:L06803
- Cox PM, Betts RA, Jones CD et al (2000) Acceleration of global warming due to carbon-cycle feedbacks in a coupled climate model. *Nature* 408:184–187
- Flanner MG, Zender CS, Randerson JT et al (2007) Present-day climate forcing and response from black carbon in snow. *J Geophys Res* 112:D11202
- Forster P, Ramaswamy V, Artaxo P et al (2007) Changes in atmospheric constituents and in radiative forcing. In: Solomon S, Qin D, Manning M, Chen Z, Marquis M, Averyt KB, Tignor M, Miller HL (eds) *Climate change 2007: the physical science basis contribution of working group I to the fourth assessment report of the Intergovernmental Panel on Climate Change*. Cambridge University Press, Cambridge
- Giorgi F, Bi XQ, Qian Y (2002) Direct radiative forcing and regional climatic effects of anthropogenic aerosols over East Asia: a regional coupled climate-chemistry/aerosol model study. *J Geophys Res* 107(D20):4439
- Giorgi F, Bi XQ, Qian Y (2003) Indirect vs. direct effects of anthropogenic sulfate on the climate of East Asia as simulated with a regional coupled climate-chemistry/aerosol model. *Clim Chang* 58:345–376
- Guo X, Fu D, Guo X et al (2014) A case study of aerosol impacts on summer convective clouds and precipitation over Northern China. *Atmos Res* 142:142–157
- Hall A, Qu X (2006) Using the current seasonal cycle to constrain snow albedo feedback in future climate change. *Geophys Res Lett* 33:L03502
- Hansen J, Nazarenko L (2004) BC climate forcing via snow and ice albedos. *Proc Natl Acad Sci* 101:423–428
- Harris I, Jones PD, Osborn TJ et al (2014) Updated high-resolution grids of monthly climatic observations—the CRU TS3.10 dataset. *Int J Climatol* 34:623–642
- Haywood JM, Boucher O (2000) Estimates of the direct and indirect radiative forcing due to tropospheric aerosol: a review. *Rev Geophys* 38:513–543
- Haywood JM, Francis P, Dubovik O et al (2003) Comparison of aerosol size distributions, radiative properties, and optical depths determined by aircraft observations and Sun photometers during SAFA RI 2000. *J Geophys Res* 108(D13):8471
- Huang NE, Wu Z (2008) A review on Hilbert–Huang transform: method and its applications to geophysical studies. *Rev Geophys* 46:RG2006
- Huang Y, Dickinson RE, Chameides WL (2006) Impact of aerosol indirect effect on surface temperature over East Asia. *Proc Natl Acad Sci U S A* 103:4371–4376

- Huang J, Guan X, Ji F (2012) Enhanced cold-season warming in semi-arid regions. *Atmos Chem Phys* 12:5391–5398
- Jacobson MZ (2004) Climate response of fossil fuel and biofuel BC, accounting for BC's feedback to snow and sea ice albedo and emissivity. *J Geophys Res* 109:D21201
- Ji F, Wu Z, Huang J et al (2014) Evolution of land surface air temperature trend. *Nat Clim Chang* 4:462–466
- Jiang Y, Liu X, Yang X et al (2013) A numerical study of the effect of different aerosol types on East Asian summer clouds and precipitation. *Atmos Environ* 70:51–63
- Koch D, Menon S, Genio AD et al (2009) Distinguishing aerosol impacts on climate over the past century. *J Clim* 22:2659–2677
- Levine JS, Cofer WR, Cahoon DR, Winstead EL (1995) Biomass burning: a driver for global change. *Environ Sci Technol* 29:120–125
- Liu PF, Zhao CS, Hallbauer E et al (2011a) Hygroscopic properties of aerosol particles at high relative humidity and their diurnal variations in the North China plain. *Atmos Chem Phys* 11:3479–3494
- Liu X, Xie X, Yin ZY et al (2011b) A modeling study of the effects of aerosols on clouds and precipitation over East Asia. *Theor Appl Climatol* 106:343–354
- Liu X, Yan L, Yang P et al (2011c) Influence of Indian summer monsoon on aerosol loading in East Asia. *J Appl Meteorol Climatol* 50:523–533
- Menon S, Hansen J, Nazarenko L, Luo YF (2002) Climate effects of black carbon aerosols in China and India. *Science* 297:2250–2253
- Qian Y, Leung RL, Ghan SJ, Giorgi F (2003) Regional climate effects of aerosols over China: modeling and observation. *Tellus B* 55:914–934
- Qian C, Yan ZW, Wu Z et al (2011) Trends in temperature extremes in association with weather–intraseasonal fluctuations in Eastern China. *Adv Atmos Sci* 28(2):297–309
- Qin Z, Zou X, Weng F (2012) Comparison between linear and nonlinear trends in NOAA-15 AMSU-A brightness temperatures during 1998–2010. *Clim Dyn* 39:1763–1779
- Ribes A, Terray L (2013) Application of regularised optimal fingerprinting to attribution. Part II: application to global near-surface temperature. *Clim Dyn* 41:2837–2853
- Ribes A, Planton S, Terray L (2013) Application of regularised optimal fingerprinting to attribution. Part I: method, properties and idealised analysis. *Clim Dyn* 41:2817–2836
- Shi Y, Gao X, Wu J et al (2011) Changes in snow cover China in the 21st century as simulated by a high resolution regional climate model. *Environ Res Lett* 6:045401
- Shine K, Fouquart Y, Ramaswamy V et al (1995) Radiative forcing. In: Houghton J, Meira Filho L, Bruce J, Lee H, Callander B, Harris N, Maskell K (eds) *Radiative forcing of climate change and an evaluation of the IPCC IS92 emission scenarios*. Cambridge University Press, Cambridge, pp 163–203
- Shiogama H, Christidis N, Caesar J et al (2006) Detection of greenhouse gas and aerosol influences in changes in temperature extremes. *SOLA* 2:152–155
- Stott PA, Stone DA, Allen MR (2004) Human contribution to the European heatwave of 2003. *Nature* 432:610–613
- Streets DG, Bond TC, Carmichael GR et al (2003) An inventory of gaseous and primary aerosol emissions in Asia in the year 2000. *J Geophys Res* 108(D21):8809
- Sun YL, Wang ZF, Fu PQ et al (2013) Aerosol composition, sources and processes during wintertime in Beijing, China. *Atmos Chem Phys* 13:4577–4592
- Sun Y, Zhang XB, Zwiers FW (2014) Rapid increase in the risk of extreme summer heat in Eastern China. *Nat Clim Chang* 4:1082–1085
- Tao R, Che HZ, Chen QL et al (2014) Study of aerosol optical properties based on ground measurements over Sichuan Basin, China. *Aerosol Air Qual Res* 14(3):905–915
- Taylor KE, Stouffer RJ, Meehl GA (2012) An overview of CMIP5 and the experiment design. *Bull Am Meteorol Soc* 93:485–498
- Wang T, Li S, Shen Y, Deng J, Xie M (2010) Investigations on direct and indirect effect of nitrate on temperature and precipitation in China using a regional climate chemistry modeling system. *J Geophys Res* 115:D00K26
- Wen HQ, Zhang X, Xu Y et al (2013) Detecting human influence on extreme temperatures in China. *Geophys Res Lett* 40:1171–1176
- Wilcox LJ, Highwood EJ, Dunstone NJ (2013) The influence of anthropogenic aerosol on multi-decadal variations of historical global climate. *Environ Res Lett* 8:024033
- Wu PP, Han ZW (2011) Modeling of the second indirect effect of anthropogenic aerosols in East Asia. *Atmos Ocean Sci Lett* 4:316–323
- Wu Z, Huang NE (2009) Ensemble empirical mode decomposition: a noise-assisted data analysis method. *Adv Adapt Data Anal* 1(1):1–41
- Wu Z, Huang NE, Wallace JM et al (2011) On the time-varying trend in global-mean surface temperature. *Clim Dyn* 37:759–773
- Xu Q (2001) Abrupt change of the mid-summer climate in Central East China by the influence of atmospheric pollution. *Atmos Environ* 35:5029–5040
- Yang Q, Bitz CM, Doherty SJ (2014) Offsetting effects of aerosols on Arctic and global climate in the late 20th century. *Atmos Chem Phys* 14:3969–3975
- Zhang X, Zwiers FW, Hegerl GC et al (2007) Detection of human influence on 20th century precipitation trends. *Nature* 448:461–465
- Zhao CS, Tie XX, Lin YP (2006) A possible positive feedback of reduction of precipitation and increase in aerosols over Eastern Central China. *Geophys Res Lett* 33:L11814
- Zhuang BL, Lia S, Wang TJ et al (2013a) Direct radiative forcing and climate effects of anthropogenic aerosols with different mixing states over China. *Atmos Environ* 79:349–361
- Zhuang BL, Liu Q, Wang TJ et al (2013b) Investigation on semi-direct and indirect climate effects of fossil fuel black carbon aerosol over China. *Theor Appl Climatol* 114:651–672